Inorg. Chem. **2008**, *47*, 11314−11323

Reversible Core-Interconversion of an Iron(III) Dihydroxo Bridged Complex

Athanassios K. Boudalis,*,†,‡ Juan Modesto Clemente-Juan,‡,§ Françoise Dahan,‡ Vassilis Psycharis,† Catherine P. Raptopoulou,† Bruno Donnadieu,‡,|| Yiannis Sanakis,† and Jean-Pierre Tuchagues*,‡

Institute of Materials Science, NCSR "Demokritos", 153 10 Aghia Paraskevi Attikis, Greece, Laboratoire de Chimie de Coordination du CNRS, UPR 8241, 205, route de Narbonne, 31077 Toulouse Cedex 04, France, Instituto de Ciencia Molecular, Universidad de Valencia, c/ Doctor Moliner, 50, 46100 Burjassot, Spain, and Department of Chemistry, University of California at Riverside, Riverside, California 92521

Received April 22, 2008

Complexes $[Fe(Hhbi)_2(NO_3)]\cdot 2EtOH$ (**1**·2EtOH) and $[Fe_2(\mu\text{-}OH)_2(Hhbi)_4]\cdot 2H_2O\cdot 8EtOH$ (**2**·$2H_2O$·8EtOH) crystallize in the orthorhombic *Fdd*2 and $P4_22_12$ space groups, respectively ($Hhbi^-$ = the monoanion of 2-(2′-hydroxyphenyl benzimidazole). Complex **1** exhibits paramagnetic relaxation as evidenced by Mössbauer spectroscopy, and significant axial zero-field splitting (1.5 $cm^1 < D < 3\ cm^{-1}$), along with a rhombic distortion ($E = 0.205\ cm^{-1}$), as shown by X-band electron paramagnetic resonance (EPR) spectroscopy. Complex **2** undergoes, upon drying, a core conversion toward an oxo-bridged diferric species and, to a smaller extent, decomposition toward a mononuclear ferric complex, as evidenced by Mössbauer, magnetic, EPR, and mass spectrometry data. The core conversion is reversible through recrystallization from wet EtOH, leading to the original complex, which crystallizes in the initial space group.

Introduction

Non-heme iron metalloproteins with mono and dinuclear active sites are involved in various biological processes.[1] On the basis of X-ray diffraction and spectroscopic studies, mononuclear non-heme iron centers are proposed to be the active species in many catalytic cycles of enzymes, including for example protocatechuate 3,4-dioxygenase (3,4-PCD),[2] lipoxygenases,[3] isopenicillin N-synthase (IPSN),[4] iron-containing nitrile hydratases,[5] and the non-heme iron of photosynthetic reaction centers.[6] Complexes of iron(II) or iron(III) bridged by oxo, hydroxo, or carboxylato ligands play a key role in the area of bioinorganic chemistry.[7] In particular, a dihydroxo-bridged diferric active site has been found in the Methane Monoxygenase of aerobic methanotrophic bacteria.[8] There has been a number of structurally characterized Fe^{III} dihydroxo bridged dinuclear complexes; these are $[FeL(OH)(H_2O)]_2$ [L^{2-} = the dianion of 2,6-pyridinedicarboxylic acid (**I**),[9] the dianion of 4-hydroxo-2,6-pyridinedicarboxylic acid (**II**),[9] the dianion of 4-dimethylamino-2,6-pyridinedicarboxylic acid (**III**)[10]], $[FeL(OH)]_2$

* To whom correspondence should be addressed. E-mail: tbou@ims.demokritos.gr.
† Institute of Materials Science, NCSR "Demokritos".
‡ Laboratoire de Chimie de Coordination du CNRS.
§ Universidad de Valencia.
|| University of California at Riverside.

(1) (a) Solomon, E. I.; Brunold, T. C.; Davis, M. I.; Kemsley, J. N.; Lee, S. K.; Lehnert, N.; Neese, F.; Skulan, A. J.; Yang, Y. S.; Zhou, J. *Chem. Rev.* **2000**, *100*, 235. (b) Costas, M.; Mehn, M. P.; Jensen, M. P.; Que, L. *Chem. Rev.* **2004**, *104*, 939–986, and references therein.
(2) (a) Ohlendorf, D. H.; Lipscomb, J. D.; Weber, P. C. *Nature* **1988**, *336*, 403–405. (b) Ohlendorf, D. H.; Orville, A. M.; Lipscomb, J. D. *J. Mol. Biol.* **1994**, *244*, 586–608.
(3) (a) Minor, W.; Steckzko, J.; Stec, B.; Otwinowski, Z.; Bolin, J. T.; Walter, R.; Axelrod, B. *Biochemistry* **1996**, *35*, 10687–10701. (b) Skrzypczak-Jankun, E.; Amzel, L. M.; Kroa, B. A.; Funk, M. O. J. *Proteins: Struct., Funct., Genet.* **1997**, *29*, 15–31.
(4) Roach, P. L.; Cliflon, I. J.; Hensgens, C. M. H.; Shibata, N.; Schofield, C. J.; Hajdu, J.; Baldwin, J. E. *Nature* **1997**, *387*, 827.
(5) (a) Huang, W.; Jia, J.; Cummings, J.; Nelson, M.; Schneider, G.; Lindqvist, Y. *Structure* **1997**, *5*, 691–699. (b) Nagashima, S.; Nakasato, M.; Dohmae, N.; Tsujimura, M.; Takio, K.; Odaka, M.; Yohda, M.; Kamiya, N.; Endo, I. *Nature Struct. Biol.* **1998**, *5*, 347–351.
(6) Deisenhofer, J.; Epp, E.; Miki, K.; Huber, R.; Michel, H. *Nature* **1985**, *318*, 618.
(7) Wallar, B. J.; Lipscomb, J. D. *Chem. Rev.* **1996**, *96*, 2625.
(8) Elango, N.; Radhakrishnan, R.; Froland, W. A.; Wallar, B. J.; Earhart, C. A.; Lipscomb, J. D.; Ohlendorf, D. H. *Protein Sci.* **1997**, *6*, 556.
(9) Thich, J. A.; Ou, C. C.; Powers, D.; Vasiliou, B.; Mastropaolo, D.; Potenza, J. A.; Schugar, H. S. *J. Am. Chem. Soc.* **1976**, *98*, 1425.
(10) Ou, C. C.; Lalancette, R. A.; Potenza, J. A.; Schugar, H. J. *J. Am. Chem. Soc.* **1978**, *100*, 2053.

10.1021/ic800716r CCC: $40.75
Published on Web 10/21/2008

Scheme 1. Ligand 2-(2′-Hydroxyphenyl)-benzimidazole (H_2hbi)

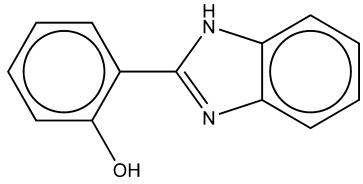

H_2hbi

(**IV**), (L^{2-} = the dianion of *N*,*N*′-ethylenebis(salicylamine)),[11] {[Fe(HL)(OH)](ClO_4)}$_2$ (**V**), (HL^- = the monoanion of (N,N′-bis(2-hydroxy-4-methylbenzene-1,2-diamethylene)diaminopropane)),[12] [Fe(H_2L)$_2$(OH)]$_2$ (**VI**), (H_2L^- = the monoanion of 4-methyl-2,6-bis(5-methylpyrazol-3-yl)phenol),[13] [FeL(OH)]$_2$ (**VII**), (L^{4-} = the tetraanion of *N*,*N*′-bis(2,3-dihydrobenzoyl)-1,4-diazabutane),[14] [Fe(HL)(OH)]$_2$ (HL^- = the monoanion of 3-methyl-5-(2-hydroxyphenyl)pyrazole) (**VIII**),[15] [FeBrL(OH)]$_2$ (**IX**) (L^- = the anion of *N*-(methoxybis-(2-pyridyl)methyl)pyridine-2-carboxamide),[16] [FeL(OH)]$_2$(NO_3)$_2$ (**X**),[17] (L^- = the anion of (2-hydroxy-5-nitrobenzyl)(2-pyridylmethyl)(2-(2-pyridyl)ethyl)amine), [Fe(HL)(OH)]$_2$(ClO_4)$_4$ (**XI**) (HL = the zwitterionic form of 2,6-bis((*N*,*N*′-bis-(2-picolyl)amino)methyl)-4-tert-butylphenol).[18]

2-(2′-Hydroxyphenyl)-benzimidazole (H_2hbi) and its derivatives are long known ligands with various uses (Scheme 1). They have been studied as laser dyes,[19] while the coordination chemistry of H_2hbi has been previously studied in conjunction with the electro-[20] and photoluminescence[21] properties of its complexes. In our area of interest, the ligand offers the simultaneous presence of one imidazole nitrogen donor, as well as one phenol oxygen donor. It is therefore of high utility in the study of non-heme iron metalloproteins, since its donor atoms can model the coordination environment of their active sites. Although the iron(III) chemistry of H_2hbi has been previously studied,[22,23] no structural study has been reported on any of its iron(III) complexes. Herein, we present the first structural studies of its iron(III) complexes, as a first step to explore its ability to model non-heme iron metalloproteins. In particular, we report the syntheses and structural studies of complexes [Fe(Hhbi)$_2$(NO_3)]·2EtOH (**1**·2EtOH) and [Fe$_2$(μ-OH)$_2$(Hhbi)$_4$]·2H_2O·8EtOH (**2**·2H_2O·8EtOH). Also, we report on a core interconversion of complex **2**, monitored by various techniques and elucidated by Mössbauer spectroscopy and magnetic susceptibility measurements.

Experimental Section

Materials and Methods. All chemicals were used as received, except 2-(2′-hydroxyphenyl)benzimidazole (H_2hbi), which was synthesized by a modification of a literature procedure.[24] **Caution!** *Although no such behavior was observed during the present work, perchlorates are potentially explosive and should be handled with care.*

(2-Hydroxyphenyl)-benzimidazole (H2hbi). *o*-Phenylenediamine (6.50 g, 60.1 mmol) and salicylic acid (8.30 g, 60.1 mmol) were added to 50 mL of H_3PO_4 and refluxed at 185 °C for 4 h. The blue-green suspension that formed was poured into 100 mL of ice water and left at 4 °C for 24 h. The light blue precipitate was then filtered and added to 75 mL of water, and the suspension that formed was neutralized with 5 M NaOH. The violet precipitate that formed when the pH reached ~7 was filtered and dried in vacuo. Yield: 1.68 g (13%).

[Fe(Hhbi)$_2$(NO_3)]·2EtOH (1·2EtOH). A solution of Fe(NO_3)$_3$·9$H_2$0 (0.20 g, 0.5 mmol) in ethanol (7 mL) was slowly added to a stirred suspension of H_2hbi (0.21 g, 1.00 mmol) in ethanol (8 mL) at room temperature. Upon addition of triethylamine (0.20 mL, 1.5 mmol), the color of this slurry turned to deep red and the suspension dissolved over minutes. The resulting solution was stirred for 1 h, filtered and left to slowly evaporate. After 36 h, X-ray quality red plates of **1**·2EtOH formed. They were collected by filtration, washed with a minimum amount of EtOH, and dried in air. Yield: 0.27 g (86%). Anal. Calcd for $C_{30}H_{30}FeN_5O_7$ (%): C, 57.34; H, 4.81; N, 11.14. Found: C, 56.7; H, 4.5; N, 11.3. IR (KBr, cm^{-1}): 1625 m, 1602 m, 1562 s, 1517 s [$\upsilon_1(A_1)_{nitrate}$], 1480 vs, 1445 s, 1401 cm^{-1} vs, 1385 s [$\upsilon_3(E')_{nitrate}$], 1248 s [$\upsilon(C-O)_{phenol}$], 1142 s, 1083 m, 1044 s, 1009 m, 985 m, 867 s, 807 s, 754 s [π(C−H)], 735 vs [π(C−H)], 620 s, 564 s, 493 s, 474 s, 426 m.

[Fe$_2$(μ-OH)$_2$(Hhbi)$_4$]·2H_2O·8EtOH(2·2H_2O·8EtOH).Method A. A suspension of H_2hbi (0.21 g, 1.00 mmol) and NEt_3 (0.28 mL, 2.00 mmol) in EtOH (5 mL) was added to a stirred solution of Fe(ClO_4)$_3$·6H_2O (0.23 g, 0.50 mmol) in EtOH (5 mL). The color of the solution changed immediately from orange to dark red-orange, and the suspension started to dissolve. The mixture was stirred for 5 min, filtered, and left undisturbed. After 2 days, X-ray quality red blocks of **2**·2H_2O·8EtOH formed. They were collected by filtration, washed with EtOH, and vacuum-dried for a few minutes. Yield: 0.25 g (75%). The dried solid analyzed as **2**·0.25H_2O. Anal. Calcd for $C_{52}H_{38.5}Fe_2N_8O_{6.25}$ (%): C, 63.27; H, 3.93; N, 11.35; Found: C, 63.26; H, 3.57; N, 11.27. IR (KBr, cm^{-1}): 1625 m, 1602 m [v(C=N)], 1557 s, 1480 vs, 1441 s, 1401 vs, 1259 s [v(C−O)$_{phenol}$], 1135 s, 1083 m, 1039 s, 1009 m, 985 m, 857 s, 807 s, 754 s [π(C−H)], 738 vs [π(C−H)], 620 s, 564 s, 493 s, 474 s, 426 m. Mass (*m*/*z*): 474 [Fe(Hhbi)$_2$]$^+$.

Drying of the same material in vacuo over silica, led to a dark red amorphous powder, yielding IR, microanalytical, and mass spectrometry data practically identical to those of the crystalline sample.

Method B. A 50 mg quantity of the amorphous dark red powder was added to EtOH (30 mL) and stirred until the solution was saturated. The undissolved solid was filtered off, and 10 mL of

(11) Borer, L.; Thalken, L.; Ceccarelli, C.; Glick, M.; Zhang, J. H.; Reiff, W. M. *Inorg. Chem.* **1983**, *22*, 1719.
(12) Nanda, K. K.; Dutta, S. K.; Baitalik, S.; Venkatsubramanian, K.; Nag, K. *J. Chem. Soc., Dalton Trans.* **1995**, 1239.
(13) Dutta, S. K.; Nanda, K. K.; Flörke, U.; Badbhade, M.; Nag, K. *J. Chem. Soc., Dalton Trans.* **1996**, 2371.
(14) Enemark, E. J.; Stack, T. D. P. *Inorg. Chem.* **1996**, *35*, 2719.
(15) Tanase, S.; Bouwman, E.; Long, G. J.; Shahin, A. M.; Mills, A. M.; Spek, A. L.; Reedijk, J. *Eur. J. Inorg. Chem.* **2004**, 4572.
(16) Zhu, S.; Brennessel, W. W.; Harrisson, R. G.; Que, L. *Inorg. Chim. Acta* **2002**, *337*, 32.
(17) Kurosaki, H.; Yoshida, H.; Ito, M.; Higuchi, E.; Goto, M. *Bioorg. Med. Chem. Lett.* **2001**, *11*, 785.
(18) Ghiladi, M.; Larsen, F. B.; McKenzie, C. J.; Sotofte, I.; Tuchagues, J.-P. *Dalton Trans.* **2005**, 1687.
(19) (a) Costela, A.; Garcia-Moreno, I. *Chem. Phys.* **1996**, *206*, 383. (b) Fellows, C. E.; Täuber, U.; Carvalho, C. E. M.; Carvalhaes, C. G. *Braz. J. Phys.* **2005**, *35*, 933. (c) Fellows, C. E.; Täuber, U.; Rodegheri, C. C.; Carvalho, C. E. M.; Acevedo, D. F.; Bertolotti, S. G.; Barbero, C. *Opt. Mater.* **2004**, *27*, 499.
(20) Hamada, Y.; Sano, T.; Fujii, H.; Nishio, Y.; Takahashi, H.; Shibata, K. *Jpn. J. Appl. Phys* **1996**, *35*, L1339.
(21) Tong, Y.-P.; Zheng, S.-L.; Chen, X.-M. *Eur. J. Inorg. Chem.* **2005**, 3734.
(22) Dubey, R. K.; Dubey, U. K.; Mishra, C. M. *Trans. Met. Chem.* **2006**, *31*, 849.
(23) Wahlgren, C. G.; Addison, A. W.; Burman, S.; Thompson, L. K.; Sinn, E.; Rowe, T. M. *Inorg. Chim. Acta* **1989**, *166*, 59.

Table 1. Crystal Data for the Described Complexes

	1·2EtOH	**2**·2H$_2$O·8EtOH
formula	$C_{30}H_{30}FeN_5O_7$	$C_{68}H_{90}Fe_2N_8O_{16}$
FW	628.44	1387.18
T (K)	160	160
crystal system	orthorhombic	tetragonal
space group	*Fdd*2	$P4_22_12$
a (Å)	32.654(7)	17.5819(13)
b (Å)	15.738(7)	17.5819(13)
c (Å)	11.161(2)	11.7959(9)
V (Å^3)	5736(3)	3646.4(5)
Z	8	2
ρ_{calc} (g cm^{-3})	1.456	1.263
λ (Å)	0.71073	0.71073
μ (mm^{-1})	0.583	0.466
h	−37 to 37	−17 to 20
k	−18 to 18	−20 to 20
l	−12 to 12	−13 to 13
refl. meas./ unique	9399/2288 (R_{int} = 0.0932)	18940/2907 (R_{int} = 0.1409)
refl. obs.	1836	2050
$R1$, $wR2^{a,b,c}$(all)	0.0624, 0.1124	0.1014, 0.2009
$R1$, $wR2$ (obs.)	0.0436, 0.1019	0.0704, 0.1816

[a] $R = \sum||F_o| - |F_c||/\sum|F_o|$. [b] $wR = [\sum w(|F_o^2| - |F_c^2|)^2/\sum w|F_o^2|^2]^{1/2}$. [c] $w = [\sigma^2(F_o^2) + (aP)^2 + (bP)]^{-1}$ where $P = (F_o^2 + 2F_c^2)/3$, with **1**: a = 0.0613, b = 0; **2**: a = 0.1268, b = 0. ($F_o > 4\sigma(F_o)$).

EtOH were added to the saturated solution. This solution was then left in a capped vial. X-ray quality crystals of **2**·2H$_2$O·8EtOH were obtained after several weeks. Yield: 10 mg (∼20%).

X-ray Crystallography. The selected crystals of **1**·2EtOH (red plate, 0.40 × 0.35 × 0.08 mm^3) and **2**·H$_2$O·2EtOH (red block, 0.35 × 0.25 × 0.10 mm^3), were mounted on a Stoe imaging plate diffractometer system (IPDS) using a graphite monochromator (λ = 0.71073 Å) and equipped with an Oxford Cryosystems cooler device. The data were collected at 160 K. The crystal-to-detector distance was 80 mm (max 2θ value 48.4°). Data were collected[25] with a φ oscillation movement (**1**·2EtOH: φ = 0.0°−249.9°, $\Delta\varphi$ = 1.7°; **2**·2H$_2$O·8EtOH: φ = 0.0°−199.5°, $\Delta\varphi$ = 1.5°). Numerical absorption corrections[26] were applied to **2**·2H$_2$O·8EtOH (T_{max} = 0.6148, T_{min} = 0.5138). The structures were solved by direct methods using SHELXS-97[27] and refined by full-matrix least-squares on F_o^2 with SHELXL-97.[28] Two ethanol molecules and one water molecule were found in the asymmetric unit of **2**·2H$_2$O·8EtOH. Disorder could be solved on an ethanol's methyl (i.e., C17) in the 0.50/0.50 ratio, which was kept isotropic as well as O5*w*. H atoms bonded to O5*w* were not found. All other non-H atoms anisotropic with a large thermal agitation on C14 and C15. H atoms were introduced in calculations with the riding model, with thermal parameters equal to 1.1 times that of the atom of attachment. Scattering factors were taken from the International Tables of Crystallography.[29] The maximum and minimum peaks on the final difference Fourier map were 0.360 and −0.351 e A^{-3} for **1**·2EtOH and 1.366 and −0.491 e A^{-3} for **2**·H$_2$O·8EtOH. Crystal data collection and refinement parameters are collected in Table 1, and selected bond distances and angles are gathered in Table 2 for **1** and **2**. **1**·2EtOH crystallized in the chiral group *Fdd*2, consequently the absolute configuration was determined through refinement of the Flack's parameter, X,[30] which reflects the polarity of the structure: $F_o^2 = (1 - X)F(h)^2 + XF(-h)^2$. The value of X was found close to zero [X = −0.01(3)] clearly indicating refinement of the appropriate enantiomer.

A crystal of **2**·2H$_2$O·8EtOH originating from recrystallization of the dried powder was mounted in a capillary on a Crystal Logic Dual Goniometer diffractometer using graphite monochromated Mo radiation. Unit cell dimensions were determined and refined by using the angular settings of 25 automatically centered reflections in the range 11°<2θ < 23°.

Physical Measurements. Microanalyses for C, H, and N were performed by the Microanalytical Laboratory of the Laboratoire de Chimie de Coordination at Toulouse. Infrared spectra (4000−400 cm^{-1}) were recorded as KBr disks and as Nujol mulls on a Perkin-Elmer Spectrum GX FT-IR spectrometer. Mass spectra (FAB$^+$) were recorded in dmf as solvent and 3-nitrobenzyl alcohol matrix with a Nermag R10-10 spectrometer. Mössbauer measurements were recorded on a constant acceleration conventional spectrometer with a 50 mCi source of ^{57}Co (Rh matrix). The absorber was a powdered sample enclosed in a 20 mm diameter cylindrical, plastic sample-holder, the size of which had been determined to optimize the absorption. Variable-temperature spectra were obtained in the 80−300 K range, by using a MD 306 Oxford cryostat, the thermal scanning being monitored by an Oxford ITC4 servocontrol device (±0.1 K accuracy). The Recoil[31] program package was used to fit the Mössbauer parameters and determine their standard deviations of statistical origin (given in parentheses). Isomer shift values (δ) are relative to iron foil at 293 K. Variable temperature (2−300 K) magnetic susceptibility data were collected on powdered microcrystalline solids on a Quantum Design MPMS SQUID susceptometer. Data were corrected with the standard procedure for the contribution of the sample holder and diamagnetism of the sample. The magnetic susceptibility has been computed by exact calculation of the energy levels associated with the spin Hamiltonian through diagonalization of the full matrix with a general program for axial symmetry.[32] Least-squares fittings were accomplished with an adapted version of the function-minimization program MINUIT.[33] The error-factor R is defined as $R = \sum(\chi_{exp} - \chi_{calc})^2/N\chi_{exp}^2$, where N is the number of experimental points. Simulations of the magnetization M versus applied field H data were carried out with the MAGPACK program package, using parameters derived from fits of the magnetic susceptibility.[34] Powder X-ray diffraction (XRD) data were collected on a D500 Siemens diffractometer equipped with a secondary graphite monochromator. X-band electron paramagnetic resonance (EPR) spectra were recorded on powdered samples of **1** (300 K) with an Elexys E500 Bruker spectrometer, and for **2** (4.2 K) with a Bruker ER 200D-SRC X-band spectrometer equipped with an Oxford ESR 9 cryostat, an NMR-Gaussmeter, and an Anritsu microwave frequency counter. EPR conditions for **1**: microwave frequency, 9.45 GHz, microwave

(24) Pla-Dalmau, A. *J. Org. Chem.* **1995**, *60*, 5468.
(25) Stoe, IPDS Manual. Version 2.93. Stoe & Cie, Darmstadt, Germany, 1997.
(26) *X-SHAPE, Crystal Optimisation for Numerical Absorption Correction*, Revision 1.01; Stoe & Cie: Darmstadt, Germany, 1996.
(27) Sheldrick, G. M. *SHELXS-97. Program for Crystal Structure Solution.*; University of Göttingen: Göttingen, Germany, 1990.
(28) Sheldrick, G. M. *SHELXL-97. Program for the refinement of crystal structures from diffraction data.* University of Göttingen: Göttingen, Germany, 1997.
(29) *International Tables for Crystallography*; Kluwer Academic Publishers: Dordrecht, The Netherlands, 1992; Vol. C, Tables 4 2.6.8 and 6.1.1.4.
(30) (a) Flack, H. D. *Acta Crystallogr., Sect. A* **1983**, *39*, 876–881. (b) Bernardinelli, G.; Flack, H. D. *Acta Crystallogr., Sect. A* **1985**, *41*, 500.
(31) Lagarec, K. *Recoil, Mössbauer Analysis Software for Windows*; http://www.physics.uottawa.ca/∼recoil.
(32) Clemente-Juan, J.-M.; Mackiewicz, C.; Verelst, M.; Dahan, F.; Bousseksou, A.; Sanakis, Y.; Tuchagues, J.-P. *Inorg. Chem.* **2002**, *41*, 1478.
(33) James, F.; Roos, M. *Comput. Phys. Commun.* **1975**, *10*, 345; MINUIT Program, a System for Function Minimization and Analysis of the Parameters Errors and Correlations.
(34) (a) Borrás-Almenar, J. J.; Clemente-Juan, J. M.; Coronado, E.; Tsukerblat, B. S. *Inorg. Chem.* **1999**, *38*, 6081. (b) Borrás-Almenar, J. J.; Clemente-Juan, J. M.; Coronado, E.; Tsukerblat, B. S. *J. Comput. Chem.* **2001**, *22*, 985.

power 63 mW, modulation amplitude 9.6 Gpp. For **2**: microwave frequency, 9.60 GHz, microwave power 50 mW, modulation amplitude 10 Gpp. Simulations of the spectra were performed by using the SpinCount package provided by Prof. M. Hendrich, Carnegie Mellon University, U.S.A.

Results and Discussion

Versatile Coordination Chemistry of 2-(2′-Hydroxyphenyl)-benzimidazole (H2hbi). The preparation of **1** may be summarized by eq 1:

$$Fe(NO_3)_3 \cdot 9H_2O + 2H_2hbi \xrightarrow{EtOH} [Fe(Hhbi)_2(NO_3)] + 2H^+ + 2NO_3^- + 9H_2O \quad (1)$$

Wahlgren et al. noted that they could only prepare dinuclear complexes formulated $[Fe_2O(Hhbi)_4]$ from the H_2hbi type of ligands,[23] while Dubey et al. reported a mononuclear and a dinuclear complex formulated [Fe(Hhbi)$(Cl)_2$] and $[Fe_2(\mu\text{-}Cl)_2(Hhbi)_4]$, respectively.[22] $[Fe(Hhbi)_2(NO_3)]$, **1**, belongs to the $[Fe(Hhbi)_2X]$ type of complex that has not been previously described. To obtain this type of mononuclear complex, a chelating anion must be involved in the room temperature synthetic procedure.

The preparation of **2** may be summarized by eq 2:

$$2Fe(ClO_4)_3 \cdot 6H_2O + 4H_2hbi \xrightarrow[NEt_3]{EtOH} [Fe_2(\mu\text{-}OH)_2(Hhbi)_4] + 6H^+ + 6ClO_4^- + 10H_2O \quad (2)$$

A similar preparation has been reported some time ago,[23] resulting in a red-brown powder formulated as $Fe_2(\mu\text{-}O)(Hhbi)_4$ and characterized by microanalytical and magnetic studies. Although no structural data were available, these results are in line with our observations (vide infra). The authors also found that for a series of similar ligands, mostly red-brown ferric species formed, which they formulated as $Fe_2(\mu\text{-}O)L_4$. Although the stoichiometry is the same as in reaction 1, a dinuclear complex results from reaction 2 because, at variance with NO_3^-, the available anion (ClO_4^-) can not play the role of chelating ligand. In addition, because reaction 2 proceeds at room temperature, the dinuclear dihydroxo species $[Fe_2(\mu\text{-}OH)_2(Hhbi)_4]$, **2**, is stabilized. But, when the same reaction is carried out under heating and in the presence of triethylorthoformate,[23] it proceeds all the way down to the final dinuclear oxo species, $Fe_2(\mu\text{-}O)(Hhbi)_4$, through dehydration. In view of the fact that such oxo-bridged diferric species are particularly stable final products, it is remarkable that the dinuclear dihydroxo species $[Fe_2(\mu\text{-}OH)_2(Hhbi)_4]$, **2**, may be regenerated through solvation of $Fe_2(\mu\text{-}O)(Hhbi)_4$ as evidenced in this study.

Mononuclear Complex [Fe(Hhbi)$_2$(NO$_3$)]·2EtOH (1·2-EtOH). The feasibility of synthesizing the $[Fe(Hhbi)_2X]$ type of complex was initially explored in view of its possible use as a model of the mononuclear non-heme iron center of enzymes. But, reactivity and catalytic studies carried out with **1** did not yield any encouraging result. However, existence of the $[Fe(Hhbi)_2X]$ type of mononuclear species has not been proven previously, which is important in view of the core conversion of the dihydroxo complex **2** into an oxo-bridged diferric species and, to a smaller extent, a mononuclear ferric $[Fe(Hhbi)_2X]$ type species.

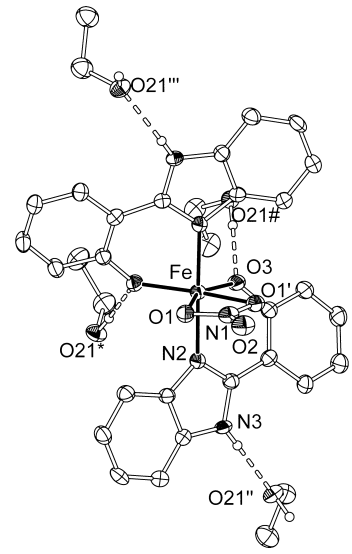

Figure 1. Partially labeled ORTEP plot of complex **1** and its hydrogen-bonded solvate molecules. For clarity, all hydrogen atoms are omitted, except those attached to the benzimidazole nitrogen atoms and the ethanolic oxygen atoms. Selected interatomic distances (Å) and angles (deg): Fe−O1 2.165(4), Fe−O3 1.890(3), Fe−N2 2.061(3), O1−Fe−O1′ 60.0(2), N1A−Fe−O1 87.2(2), N2−Fe−O1′ 90.5(2), O1A−Fe−O1 152.7(1), O3′−Fe−O1 93.5(2), N2−Fe−O3′ 94.6(1), N2−Fe−N2′ 177.2(3), O3−Fe−O3′ 113.6(2), O3−Fe−N2 87.0(1), O21#···O3 2.750, HO21#···O3 1.870, O21#−HO21···O3 176.4°, N3···O21″ 2.759, HN3···O21″ 2.050 Å, N3−HN3···O21″ 170.0°. Symmetry operations: ′ = −*x*, −*y*, *z*, ″ = 0.5 − *x*, −*y*, 0.5 + *z*, ‴ = −0.5 + *x*, *y*, 0.5 + *z*, # = 0.25 − *x*, −0.25 + *y*, 0.75 + *z*, * = −0.25 + *x*, 0.25 − *y*, 0.75 + *z*.

Description of the Structure. A partially labeled Oak Ridge Thermal Ellipsoid Plot (ORTEP) view of complex **1**, $[Fe(Hhbi)_2(NO_3)]$, is shown in Figure 1 with selected interatomic distances and angles. Complex **1** includes a single Fe^{III} cation with an O_4N_2 coordination sphere of distorted octahedral geometry brought by two bidentate $Hhbi^-$ and one bidentate NO_3^- ligands. The molecule resides on a 2-fold axis of symmetry passing through the Fe^{III} and atoms N1 and O2 of the bidentate NO_3^- ligand. As a result, the N donors of the $Hhbi^-$ ligands are in *trans* relative positions, while their O donors are in *cis* relative positions. Complex **1** participates in a three-dimensional network of hydrogen-bonds with the EtOH solvate molecules (Supporting Information, Table S2).

IR Spectrum of Complex 1. The main absorptions in the IR spectrum of complex **1** along with their assignments are given in the experimental section. The group of absorptions between 1450 and 1630 cm^{-1} is attributed to the ν(C═C) and ν(C═N) stretching vibrations of the phenolato and benzimidazolyl rings, while a peak at ∼1250 cm^{-1} is attributed to the C−O stretching vibration of the phenolato oxygen of $Hhbi^-$. Two bands at ∼754 and 736 cm^{-1} are attributed to the [π(C−H)] out-of-plane C−H bending. The ν_3(E′) and [υ_1(A$_1$)] vibrations of the bidentate nitrate are characterized by absorptions at 1385 and 1517 cm^{-1}, respectively.[35]

Mössbauer Characteristics of Complex 1. Mössbauer spectra from solid samples of **1** recorded at 4.2 and 80 K (Figure 2) exhibit broad quadrupole-split doublets attributed

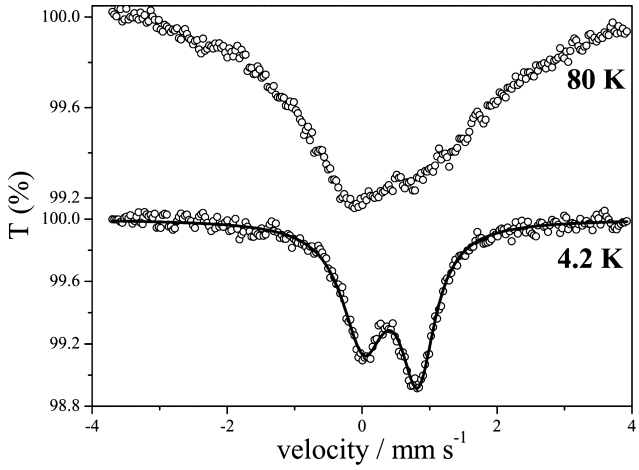

Figure 2. Mössbauer spectra of complex **1** at 80 and 4.2 K. The solid line corresponds to a fit to an asymmetric quadrupole-split doublet (see text).

to intermediate paramagnetic relaxation. The broadening is more severe for the 78 K spectrum, whereas the 4.2 K spectrum exhibits a rather well resolved asymmetric doublet. This temperature dependence of the broadening effects is usual when the high-spin ferric ion experiences appreciable zero-field splitting (zfs).[36] The behavior observed for **1** suggests a positive value for the zfs parameter, D. The 4.2 K spectrum could be fitted by an asymmetric quadrupole-split doublet ($\delta = 0.42$ mm s^{-1}, $\Delta E_{QA} = 0.80$ mm s^{-1}, $\Gamma_+ = 0.31$ mm s^{-1}, $\Gamma_+/\Gamma_- = 1.25$).

Magnetic Properties of Complex 1. Variable temperature magnetic susceptibility data of complex **1** are shown in Supporting Information, Figure S3: the $\chi_M T$ product at 300 K is 4.7 cm^3 mol^{-1} K, close the theoretical value for one high-spin Fe^{III} ion. The $\chi_M T$ product decreases very smoothly with temperature, down to 4.4 cm^3 mol^{-1} K at 14 K, and then sharply drops to 0.6 cm^3 mol^{-1} K at 1.9 K. These data are typical of an $S = 5/2$ ion with $g = 2$, exhibiting zero-field and Zeeman splitting inside the magnetic field. The hydrogen bonding network revealed by the crystal structure of the complex suggests the presence of weak intermolecular interactions. Given the fact that these two factors are manifested over the low temperature range, fits to the data were inconclusive because of correlations of the variables and will therefore not be presented.

EPR Spectrum of Complex 1. The X-band EPR spectrum from a powder sample of **1** at 300 K is shown in Figure 3 along with the effective g-values corresponding to the absorptions. The spectrum may be interpreted assuming an Fe^{III} ($S = 5/2$) species characterized by axial (D) and rhombic (E) distortions. On the basis of the Mössbauer relaxation properties discussed earlier, $D > 0$. Theoretical simulations indicate that this signal is consistent with 1.5 cm^{-1} < D < 3.0 cm^{-1}. To reproduce the line shape of the rest of the signals a rather large intrinsic line width σ_B for each transition has to be considered. This large intrinsic width is most probably due to fast relaxation effects.

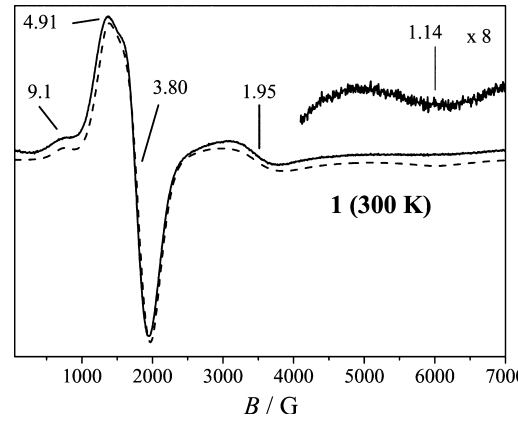

Figure 3. X-band EPR spectrum from powdered samples of **1** at 300 K. The dashed line is a theoretical simulation of the X-band EPR spectrum of complex **1** obtained for $D = +2$ cm^{-1}, $E/D = 0.205$ cm^{-1}, $\sigma_B = 150$ G, $g = 2.0$, and a Gaussian distribution on E/D of width $\sigma_{E/D} = 0.015$. The $g = 1.14$ region of the experimental spectrum is magnified by a factor of 8.

Dihydroxo Bridged Complex [Fe$_2$(μ-OH)$_2$(Hhbi)$_4$]·2H$_2$O·8EtOH (2·2H$_2$O·8EtOH) and its Reversible Core-Interconversion to an Oxo Bridged Fe$_2$(μ-O)(Hhbi)$_4$ Type Species. Description of the Structure. A partially labeled ORTEP plot of complex **2**, [Fe$_2$(μ-OH)$_2$(Hhbi)$_4$], is presented in Figure 4 with selected interatomic distances and angles. Complex **2** crystallizes in the tetragonal space group $P4_22_12$. The complex contains two iron(III) ions connected by two hydroxo bridges. The coordination sphere for each site is completed by two chelating Hhbi$^-$ ligands coordinated through one phenoxo oxygen and one imidazolyl nitrogen atoms. All oxygen donors occupy equatorial positions with respect to the plane of the Fe$_2$O$_2$ core, whereas the nitrogen donors occupy the axial coordination sites.

The coordination geometry around the iron atoms is slightly distorted octahedral. The bond lengths show a significant dispersion, covering the 1.964(4)−2.114(5) Å range. By virtue of symmetry, Fe−O(1) = Fe−O(1″) = 2.000(3) Å and Fe−O(2) = Fe−O(2′) = Fe−O(2″) = Fe−O(2‴) = 1.965(4) Å.

The intermolecular structural organization is determined by a number of hydrogen bonds between the complex and the crystallization solvents (eight EtOH and two H$_2$O molecules). These interactions create a complex network, a portion of which is sketched in Figure 5.

Powder X-ray Diffraction of the Desolvated Crystals of 2 and Single-Crystal X-ray Diffraction of the Recrystallized Powder. Although complex **2** appears as bright red crystals, upon drying it rapidly deteriorates to a dark red amorphous powder. The crystallinity of the powder, examined by powder X-ray diffraction, revealed no diffraction pattern. The low activation energy of this process (no heating or grinding being necessary) suggests that the crystal lattice is unstable outside the mother liquor and collapses because of solvent loss at room temperature.

Conversely, recrystallization of this amorphous compound in wet EtOH reconstitutes the same crystal network, as revealed by single-crystal X-ray diffraction of the recrystallized solid. Unit cell determination showed not only that the same product is obtained but also that it also crystallizes in

(35) Nakamoto, K. *Infrared and Raman Spectra of Inorganic and Coordination Compounds*, 4th ed.; Wiley: New York, 1986; pp 121−125, 254, 256 and 257.
(36) Blume, M. *Phys. Rev. Lett.* **1967**, *18*, 305.

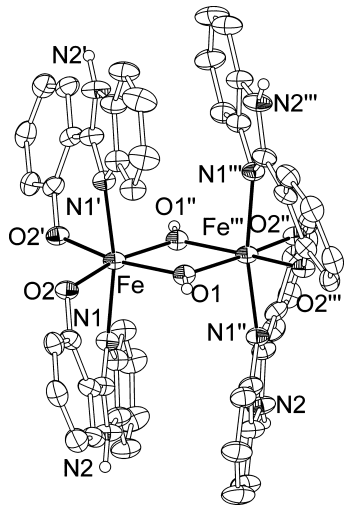

Figure 4. Partially labeled ORTEP plot of complex **2**. For clarity, hydrogen atoms are omitted, except the hydroxo ones and those attached to the benzimidazolyl nitrogen atoms. Selected interatomic distances (Å) and angles (deg): Fe−O1 2.000(3), Fe−O1″ 2.001(3), Fe−O2 1.964(4), Fe−O2′ 1.964(4), Fe−N1 2.114(5), Fe−N1′ 2.114(5), O1−Fe−O2 92.93(17), O2−Fe−N1′ 88.9(2), O1−Fe−N1 95.82(16), O2−Fe−O1″ 166.52(18), O1−Fe−O2′ 166.52(18), N1−Fe−O2′ 88.9(2), O1−Fe−N1′ 93.20(15), N1−Fe−N1′ 168.7(3), O1−Fe−O1″ 74.2(2), N1−Fe−O1″ 93.20(15), O2−Fe−N1 83.9(2), O2′−Fe−N1′ 83.9(2), O2−Fe−O2′ 100.1(3), O2′−Fe−O1″ 92.93(17), N1′−Fe−O1″ 95.81(16), Fe−O1−Fe‴ 105.8(2). Symmetry operations: ′ = $-y + 1, -x + 1, -z$; ″ = $y, x, -z$; ‴ = $-x + 1, -y + 1, z$.

the same space group, with almost identical unit cell parameters ($a = b = 17.766(8)$, $c = 11.861(6)$ Å, $V = 3744(3)$ Å^3, $T = 293(2)$ K). The structure of **2** presents striking resemblance to those of the Al^{III} and In^{III} complexes of H_2hbi previously reported.[37] What is even more surprising is that the three complexes are isostructural, the unit cell dimensions of the Al^{III} and In^{III} analogues (tetragonal $P4_22_12$ space group, $a = b = 17.603$, $c = 11.848$ Å) being very close to those of **2**. This finding suggests that this particular packing is of special stability for complex **2** and its Al^{III} and In^{III} analogues. Given the additional data presented below for complex **2**, we conclude that this packing is not simply a very stable one for this given type of structure but that it is probably crucial for the stability of the complex itself.

IR Spectra of Complex 2. The IR spectrum of complex **2** is very similar to that of **1**, the main features being attributed to the $Hhbi^-$ ligand. The main absorptions along with their assignments are given in the experimental part. The most prominent difference between the spectra of **1** and **2** stems from the $\nu_3(E')$ and $[\nu_1(A_1)]$ vibrations of the coordinated bidentate nitrate, absent in **2**, while the rest of the bands appear in the same regions. While the Fe−O−Fe absorptions are of high diagnostic value in oxo-bridged diferric complexes, because of the complexity of the spectra in the 500−800 cm^{-1} region, assignment of the Fe−O−Fe vibrations was not possible. Spectra of complex **2** recorded either as KBr disks, or as Nujol mulls, were practically identical for both the crystalline (bright red) and the dried (dark red-brown) samples. This observation led us to conclude that either both species exhibit precisely the same IR spectra or they decompose to the same product during sample preparation. However, grinding the samples with KBr and pressing them into pellets did not affect the samples more than preparing Nujol mulls.

(37) Tong, Y.-P.; Zheng, S.-L.; Chen, X.-M. *Aust. J. Chem.* **2006**, *59*, 653.

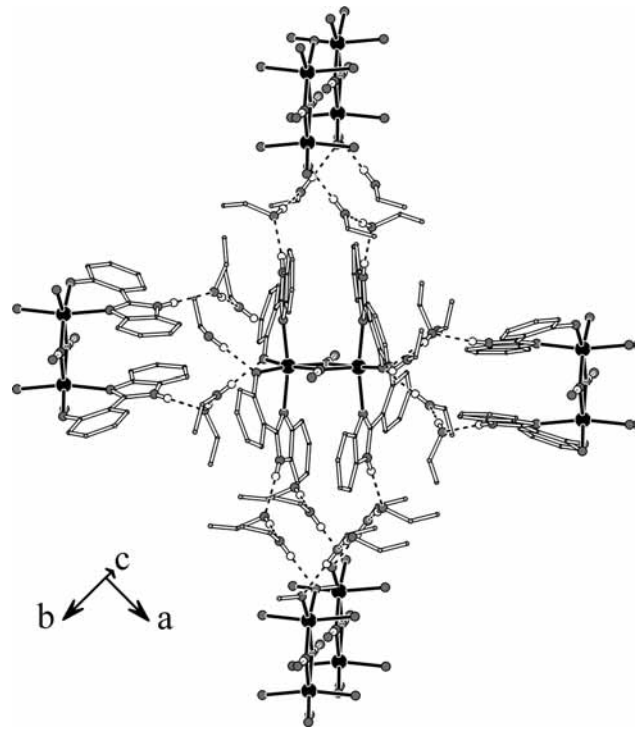

Figure 5. Portion of the crystal lattice of **2**, showing the complex hydrogen-bond network. For clarity, hydrogen atoms have been omitted to the exception of the H-bonded ones. Selected interatomic distances (Å) and symmetry operations: $O1_{hydroxo}\cdots Ow5$ (x, y, z) 3.22(2), $N2_{benzimidazolyl}\cdots O4_{ethanol}$ (x, y, z) 2.797(8), $O3_{ethanol}\cdots O2_{phenoxo}$ (x, y, z) 2.706(8), $O4_{ethanol}\cdots O3_{ethanol}$ ($x + 1/2, -y + 3/2, -z - 1/2$) 2.640(8).

Mass Spectra of Crystalline and Dried Samples of Complex 2. Both crystalline and dried samples of **2** yielded very similar mass spectra dominated by a peak at $m/z = 474$, corresponding to the mononuclear cationic fragment $[Fe(Hhbi)_2]^+$ (MW = 474.30). All other peaks corresponding to different fragments were ∼100 times weaker. This finding suggests that complex **2** has a high propensity to decompose to mononuclear species, both in its crystalline and in its amorphous (dried) forms.

Mössbauer Spectroscopy of Crystalline and Dried Samples of Complex 2. Data presented thus far suggest that complex **2** appears in two different forms in the solid state, that is, as a bright-red crystalline solid or as a dark red-brown amorphous powder. These two forms exhibit almost identical analytical, IR, and mass spectrometry data. This would suggest that they are composed either of the same material, with the color difference stemming from the grain size and texture of the solid, or of different materials, the differences of which are not discernible with these techniques. The most compelling data for answering this question were available through ^{57}Fe Mössbauer spectroscopy.

On the basis of the crystal structure of complex **2**, a unique quadrupole-split doublet would be expected. The spectrum of a sample consisting in ground microcrystals, however, revealed the existence of two doublets **A** and **B**, in an

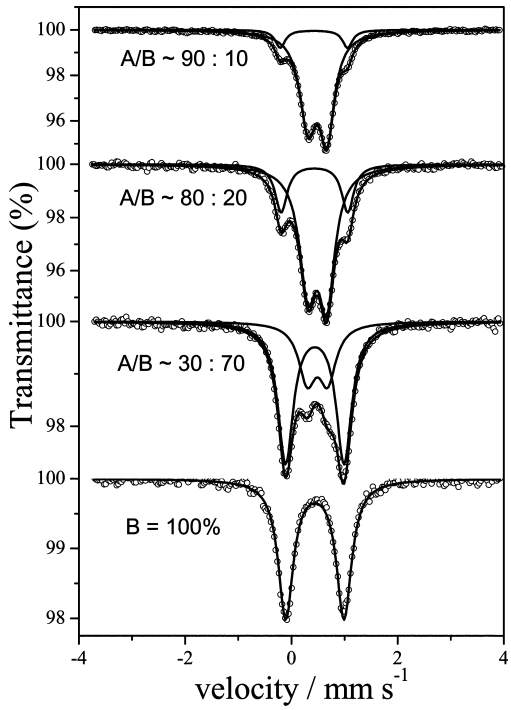

Figure 6. 80 K Mössbauer spectra for samples of **2** having undergone increasing degrees of drying (from top to bottom).

approximate 80:20 ratio, respectively, (Figure 6) and with parameters characteristic of high-spin iron(III). These doublets present similar isomer shifts (δ) but quite different quadrupole splittings (ΔE_Q) ($\delta_A = 0.49$ mm s^{-1}, $\Delta E_{QA} = 0.36$ mm s^{-1}, $\delta_B = 0.44$ mm s^{-1}, $\Delta E_{QB} = 1.10$ mm s^{-1}, at 80 K). For both doublets, a decrease of the isomer shift values with increasing temperature is attributed to a second-order Doppler effect.[38] As for the ΔE_Q values, we observe a net increase for doublet **A** upon increasing temperature, from 0.36 to 0.40 mm s^{-1}, whereas for doublet **B** there is no clear trend, the ΔE_Q value being relatively constant around 1.09 mm s^{-1}, within experimental errors (Table 2).

The most straightforward interpretation of these results being the presence of an impurity, we repeated the synthesis of complex **2** in an attempt to obtain it in a purer form: this time the crystals were vacuum-dried before being ground to prepare the Mössbauer sample. The result was that doublet **A** of the Mössbauer spectrum displayed a dramatic decrease of intensity, with a relative **A/B** ratio of 30:70 (Figure 6). All other factors being unchanged, we suspected that there might be a relation between the degree of drying and the identity of our product. To prove this beyond doubt, we recorded the spectra of (i) a fully desolvated (vacuum-dried over several days), finely ground sample and (ii) a crystalline sample that was left to dry in air for only few minutes and packed in the sample holder without grinding. Indeed, for the former sample the **A** doublet totally disappeared and only doublet **B** was observed, whereas for the latter both doublets were observed but in a **A/B** ratio of 90:10, see Figure 6.

Besides single-crystal X-ray crystallography, the identity of the product derived from recrystallization (see Experimental Section, Method B) was also verified by Mössbauer

(38) Greenwood, N. N.; Gibbs, T. C. *Mössbauer Spectroscopy*; Chapman and Hall: New York, 1971; pp. 50−53, pp 72−76.

Table 2. Mössbauer Parameter Values for the Solvated (**A**) and Desolvated (**B**) Species of Complex **2**

Iron Site	T/K	δ^b/mm s^{-1}	ΔE_Q/mm s^{-1}	$\Gamma_{1/2}$	Γ_-/Γ_+	*A* %
A[a]	80	0.489(3)	0.356(5)	0.179(6)	1.08(3)	78(2)[a]
A[a]	150	0.463(6)	0.37(2)	0.24(2)	1.17(5)	75(5)[a]
A[a]	293	0.384(9)	0.40(2)	0.23(3)	1.15(7)	79(9)[a]
B[a]	80	0.442(4)	1.098(7)	0.172(5)	1	100
B[a]	150	0.416(4)	1.098(8)	0.173(6)	1	100
B[a]	293	0.341(9)	1.08(2)	0.19(1)	1	100

[a] For higher precision, the parameters of site **A** originate from fits of the spectra obtained from the pellet containing 80% of **A**, and for site **B** from the pellet containing 100% of **B**. [b] Referenced to metallic iron foil at 300 K.

spectroscopy (Supporting Information, Figure S4). Bright-red unground crystals yielded a spectrum consisting of the same two doublets in a 80:20 ratio. The propensity of samples of **2** derived from recrystallization to decompose to the oxo-product is identical to that of the freshly prepared complex **2** prepared according to Method A.

Having thus established the effects of drying and grinding on the properties of our samples, it remained to identify the solvated and desolvated species. A survey of the literature indicates that dinuclear complexes containing the $[Fe_2(\mu\text{-}OH)_2]^{4+}$ core yield quadrupole-split doublets with isomer shifts similar to those of **A** and quadrupole splittings in the area of 0.2−0.4 mm s^{-1}. This supports the conclusion that doublet **A** corresponds to the crystallographically characterized Fe^{III} site. Moreover, this is a logical conclusion because the species detected when only a minimum amount of crystals is desolvated by drying or grinding should be the one identified by single crystal X-ray determination. However, the fact that a 10% decomposition of **2** occurred, despite the serious precautions taken to avert desolvation, suggests that the crystals are very unstable, that is, pure **2** is very difficult to obtain. This observation also sheds doubts on the validity of IR and/or microanalytical data of the "crystalline" samples. The experimental procedure to obtain these data renders sample desolvation quite likely. It is therefore probable that these data rather correspond to a mixture of the desolvated solid and complex **2**. Another important conclusion that stems from Mössbauer spectroscopy is that the color change originally observed should be associated with a chemical modification of **2**, since the marked change in the quadrupole splittings suggests an important structural distortion of the ferric site.

As for the species corresponding to doublet **B**, we observe that (a) the isomer shifts of both species are very close, whereas (b) their respective quadrupole splittings are very different; (a) suggests that donor atoms and ligands around each iron atom are the same or very similar, while (b) indicates that it is rather the symmetry of the ligand field that changes, as expressed by the quadrupole splitting. These observations turned us to suppose that an intramolecular reaction had yielded a product with a composition similar to that of **2**, but with different Mössbauer properties—possibly an oxo-bridged species. Indeed, an oxo-bridged complex would exhibit a very short Fe−O bond, which would increase the electric-field gradient around the ferric site, and consequently ΔE_Q. It has been previously shown that Mössbauer spectroscopy is very sensitive in distinguishing between oxo and hydroxo-bridged ferric sites through differ-

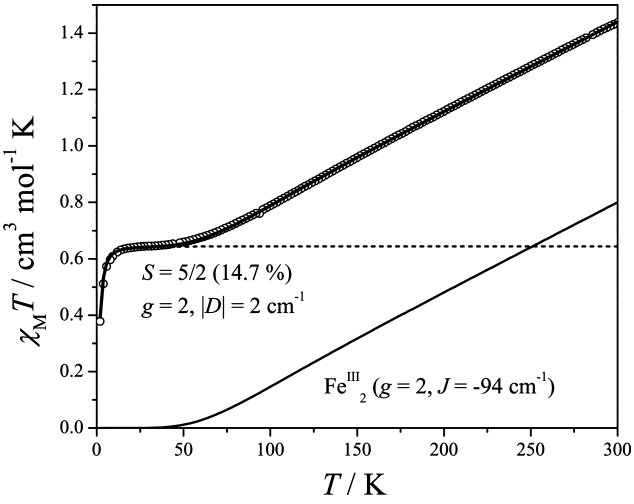

Figure 7. $\chi_M T$ vs T experimental data and fit (heavy line) for a fully dried sample of **2**. The two components of the calculated curve are shown (dimer, continuous line; paramagnetic impurity, dashed line).

ences in their quadrupole splittings.[39] To summarize, the Mössbauer parameters of doublets **A** and **B** are in agreement with those of other characterized dihydroxo bridged[11,18] and oxo-bridged ferric species, respectively.[40] It is then quite probable that a water molecule (from one OH^- bridge and one H^+) is formed and expelled from the dihydroxo bridged complex, to yield an oxo-bridged species. Analysis of the magnetic susceptibility data further supports this hypothesis (see Magnetic Properties).

In contrast to the symmetrical doublet **B**, a noteworthy feature of these spectra is the asymmetry of doublet **A**, which is better observed in the less desolvated spectra, at higher temperatures. Complexes of similar structure[11,41] exhibit a similar asymmetry which has been attributed to relaxation effects related to the occupation of the excited states with (S_{tot} = 1, 2, 3, 4, 5).[41] Doublets **A** of the 90:10 and 80:20 spectra were fitted as asymmetric doublets, with the $\Gamma_{1/2}$ value of each Lorentzian line allowed to vary independently, but with equal areas, assuming that the asymmetry stems only from the reasons stated above, and not from anisotropy of the recoilless fraction like in the Goldanskii−Karyagin effect.[38] The resulting fits were of very good quality, suggesting that our choice to take into account only the first two phenomena, and not the latter one, was valid. In addition, it was observed that the Γ_-/Γ_+ ratio shows an overall increase with increasing temperature, in agreement with a higher population of paramagnetic states, and thus a more intense anisotropy and/or relaxation.

Magnetic Properties of Crystalline and Dried Samples of Complex 2. Taking into consideration the effect of desolvation evidenced by the Mössbauer spectra of **2**, magnetic susceptibility measurements were carried out both on a fully desolvated and ground sample (Figure 7) and on a crystalline sample (Figure 8) of complex **2**. To avoid

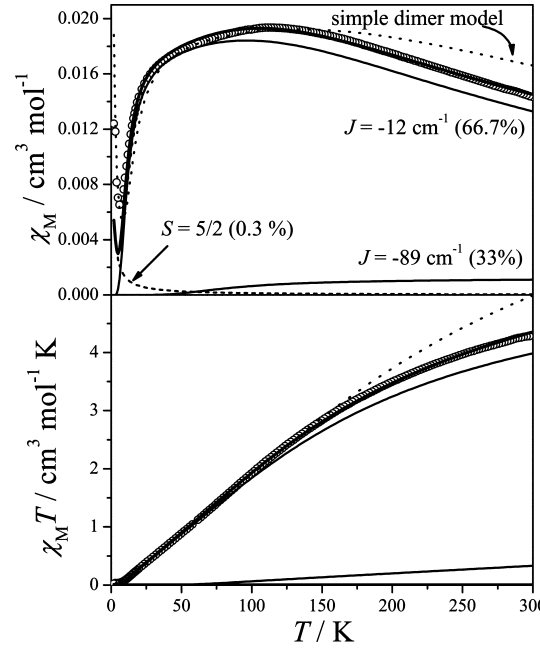

Figure 8. χ_M vs T and $\chi_M T$ vs T experimental data for a crystalline sample of **2** and calculated curves as described in the text. The heavy line is analyzed to its three components (dimers, continuous lines; paramagnetic impurity, dashed line). For comparison, the dotted line shows the best fit to a simple dimer.

deterioration, the crystals were not pressed into pellets but measured as a polycrystalline sample.

For the fully desolvated sample, the $\chi_M T$ product at 300 K is 1.44 cm^3 mol^{-1} K, while the theoretical value for two non-interacting high-spin Fe^{III} ions is 8.76 cm^3 mol^{-1} K (Figure 7). This indicates strong antiferromagnetic interactions. As the temperature drops, the $\chi_M T$ product shows a rapid decrease, reaching a plateau of ∼0.64 cm^3 mol^{-1} K around 25 K, and then sharply drops to 0.38 cm^3 mol^{-1} K at 2 K. This plateau suggests the presence of a significant fraction of ferric (S = 5/2) paramagnetic impurity. The drop below 25 K is associated with Zeeman splitting of this paramagnetic impurity in the magnetic field, along with possible zfs effects.

The data were fitted above 70 K considering a simple exchange-coupled dimer, along with a ferric paramagnetic impurity fraction, ρ. The Hamiltonian used was $\hat{H}_{dim} = -2J\,\hat{\mathbf{S}}_1\hat{\mathbf{S}}_2$, yielding $J = -94$ cm^{-1}, $g = 2.0$ (fixed), $\rho = 14.7\%$, with $R = 2.6 \times 10^{-6}$. We then calculated the behavior of the sample over the 2−300 K range. The contribution of the paramagnetic impurity was calculated by taking into account the Zeeman splitting of the S = 5/2 multiplet in the magnetic field and a zfs term (D). The Hamiltonian for the paramagnetic impurity was thus $\hat{H}_{par} = D\hat{S}_z^2 + g\beta\mathbf{H}\hat{\mathbf{S}}$. Excellent results were obtained for $J = -94$ cm^{-1}, $g = 2.0$ (fixed), $\rho = 14.7\%$ (fixed), and $|D|_{par} = 2$ cm^{-1} ($R = 2.6 \times 10^{-7}$). The value of J is typical of oxo-bridged diferric complexes[40] and supports the conclusion that an oxo species is produced upon drying of the sample. The very high amount of paramagnetic impurity is also significant, as it suggests that, apart from the formation of an oxo product, there is a secondary chemical process leading to a mononuclear paramagnetic species. This finding is in line with the mass spectrometry results, which indicate a high propensity of **2** to

(39) Boudalis, A. K.; Lalioti, N.; Spyroulias, G. A.; Raptopoulou, C. P.; Terzis, A.; Bousseksou, A.; Tangoulis, V.; Tuchagues, J.-P.; Perlepes, S. P. *Inorg. Chem.* **2002**, *41*, 6474.
(40) Kurtz, D. M. *Chem. Rev.* **1990**, *90*, 585.
(41) Cianchi, L.; Del Giallo, F.; Lantieri, M.; Moretti, P.; Spina, G.; Caneschi, A. *Phys. Rev. B* **2004**, *69*, 014418.

decompose to mononuclear species. The fitting results have been corroborated with simulations of the magnetization isotherm of complex **2** at 300 K (Supporting Information, Figure S5).

We should also note that the value of the paramagnetic impurity fraction assumes equal molecular weights for the dimer and the monomeric impurity, which however is not the case. If we consider that the molecular weight of the paramagnetic impurity is about half that of the dinuclear complex, then in terms of total iron, the paramagnetic impurity should be about 8%. For a total Mössbauer effect of ~2% (Figure 6, bottom spectrum), this would imply a Mössbauer effect of ~0.16% for the paramagnetic impurity, possibly suffering from relaxation broadening (see Mössbauer spectrum of complex **1**, Figure **2**). Thus, although the paramagnetic impurity is clearly monitored by magnetic susceptibility measurements, it may not be discernible by Mössbauer spectroscopy because of overlapping with the major doublet corresponding to the diferric species.

For the crystalline sample (Figure 8), the $\chi_M T$ value at 300 K is 4.30 $cm^3\ mol^{-1}$ K, lower than theoretically expected for two non-interacting $S = 5/2$ spins (8.76 $cm^3\ mol^{-1}$ K, $g = 2$). This indicates the interplay of antiferromagnetic interactions, weaker however than those previously observed. This is corroborated by the constant drop of the $\chi_M T$ product upon cooling (0.023 $cm^3\ mol^{-1}$ K at 2 K) and by a broad maximum of the χ_M versus T curve around 114 K. A sharp rise of the χ_M versus T curve below 6 K is attributed to a small fraction of high-spin ferric paramagnetic impurity. Initial attempts to fit these data by using a dimer model of coupled $S = 5/2$ spins yielded poor results. In agreement with the Mössbauer spectroscopy results, it was then considered that despite all precautions taken to avoid desolvation of the crystalline sample, this may have nonetheless occurred, for example, upon drying and/or purging of the sample inside the SQUID magnetometer. Therefore, a model considering two distinct antiferromagnetically coupled dimers was considered to take into account both species.

The expression used to fit the data was

$$\chi_{tot} = (1 - \alpha - \rho)\chi_{hydroxo} + \alpha\chi_{oxo} + \rho\frac{Ng^2\beta^2}{3kT}S(S+1) \quad (3)$$

where each partial susceptibility is calculated by the analytical expression[42]

$$\chi_i = \frac{2Ng_i^2\beta^2}{kT}\frac{e^{x_i} + 5e^{3x_i} + 14e^{6x_i} + 30e^{10x_i} + 55e^{15x_i}}{1 + 3e^{x_i} + 5e^{3x_i} + 7e^{6x_i} + 9e^{10x_i} + 11e^{15x_i}} \quad (4)$$

where

$$x_i = 2J_i/kT \quad (5)$$

Initial fits were carried out over the 50−300 K range, to avoid contributions of the paramagnetic impurity, while g_{oxo} and $g_{hydroxo}$ were both fixed to 2. Thus, the only free variables were $J_{hydroxo}$, J_{oxo}, and α. Fitting of the data yielded $J_{hydroxo} = -12\ cm^{-1}$, $J_{oxo} = -89\ cm^{-1}$, and $\alpha = 33\%$ ($R = 4.8 \times 10^{-5}$). The value of $J_{hydroxo}$ falls well within the range previously reported for hydroxo bridged diferric complexes containing the $\{Fe_2(OH)_2\}^{4-}$ core (−8 to −15 cm^{-1}, $H = -2JS_iS_j$ formalism). The value of J_{oxo} is typical of oxo-bridged diferric complexes as mentioned above. It is also very close to the J value independently derived for the fully dried sample. Although the value of the fraction α may not be very accurate, it indicates that, despite all precautions taken, partial desolvation did occur, leading to an oxo-bridged species.

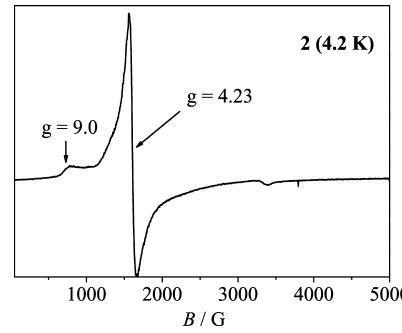

Figure 9. X-band EPR spectrum from a powdered sample of **2** at 4.2 K.

When the 2−300 K range was considered, the amount of paramagnetic impurity could not be fitted satisfactorily, but it was estimated to be less than 1%. In Figure 8, we show a calculated curve considering a 0.3% fraction of paramagnetic impurity.

EPR Spectrum of Complex 2. A spectrum of complex **2** recorded at 4.2 K is shown in Figure 9. The spectrum consists of a relatively strong derivative signal at $g = 4.23$ and a weaker absorption at $g \sim 9.0$. These signals are consistent with an $S = 5/2$ system for which zfs lifts the 6-fold degeneracy to three non-Kramers doublets. This spectrum corresponds to the ferric paramagnetic impurity fraction (14.7%) previously determined (see Magnetic Properties section). For $|D| > h\nu$ (~0.3 cm^{-1} at X-band) the feature at $g = 9.0$ is attributed to the $|\pm 1/2\rangle$ doublet whereas the absorption at $g \sim 4.23$ is attributed to the $|\pm 3/2\rangle$ doublet. The relative intensities of these signals at 4.2 K suggest a negative sign for D with $|D| \sim 1-2\ cm^{-1}$ in reasonable agreement with the results from the magnetic measurements. The relatively broad lines of the signals suggest relatively wide distributions of the zfs parameters D and/or E/D.[43]

Thermogravimetric Studies of Crystalline and Dried Samples of Complex 2. TGA experiments on both samples (Supporting Information, Figure S6) revealed that larger amounts of solvent were released from the solvated sample. The release, however, took place gradually over the 50 to 250 °C temperature range, without clear separation for the two solvents (EtOH and H_2O) as a function of increasing temperature. Consequently, the experiments could not clearly distinguish desolvation from decomposition of the hydroxo bridge to an oxo one. This agrees with our reasoning where we propose that lattice collapse due to solvates loss triggers the decomposition of the dihydroxo bridge to an oxo one. As the two phenomena follow in close succession, they are very difficult to distinguish.

(42) Kahn, O. *Molecular Magnetism*; VCH Publishers Inc.: New York, 1993; p 114.

Scheme 2. Reversible Core Conversion between a Hydroxo- And an Oxo Bridged Species

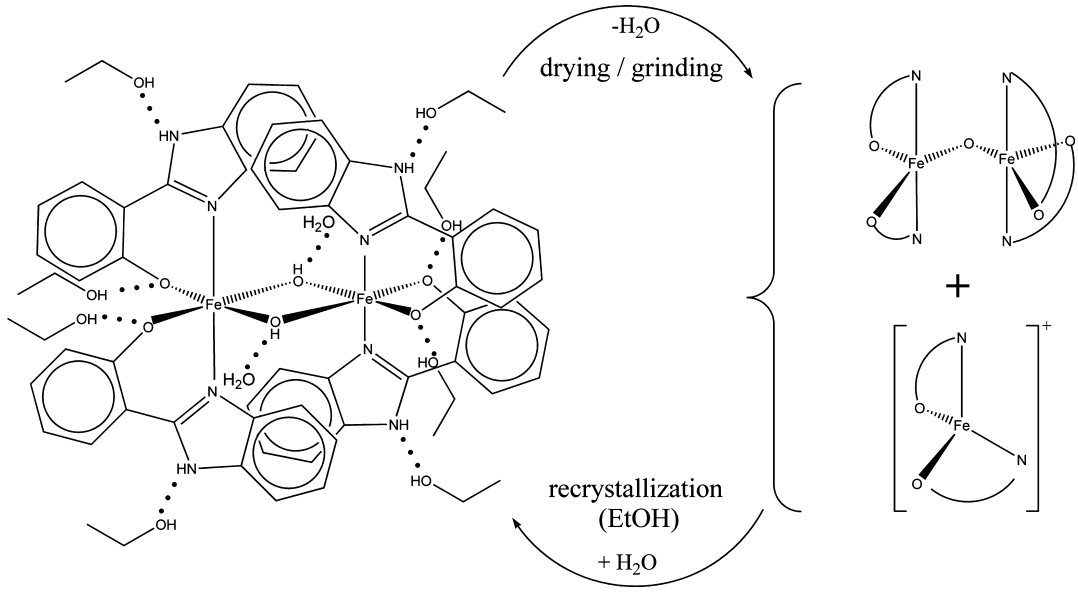

Conclusions

Mössbauer, magnetic, and EPR studies indicate that complex **2** undergoes a rare core conversion from hydroxo- to oxo-bridged, along with a partial decomposition to mononuclear paramagnetic species. In particular, Mössbauer studies on several samples of **2**, revealed a dependence of the progress of this conversion on the degree of drying. Magnetic susceptibility data corroborated this conclusion by revealing a major species with a moderate exchange interaction for the crystalline product, corresponding to a hydroxo complex. A species with a strong antiferromagnetic interaction was detected both for the crystalline sample (as a minor product) and for the dried sample (as a major product). In the latter case, this was accompanied by the appearance of a paramagnetic species, attributed to partial decomposition of the dimeric species. Formation of this paramagnetic product was also supported by EPR data in the solid state. Mass spectrometry data were also supportive of the propensity of the dimeric species to decompose to mononuclear ones.

Recrystallization experiments revealed the reversible nature of this core conversion (Scheme 2). The crystal lattice of **2**·2H_2O·8EtOH is reconstituted upon recrystallization from EtOH. The dependence of the degree of decomposition on the degree of drying suggests a structural instability of complex **2** which is compensated by the high stability of the crystal lattice of **2**·2H_2O·8EtOH: once the crystal lattice starts collapsing, the complex begins to decompose. Conversely, when the conditions (during recrystallization) allow formation of the crystal lattice, it is reconstituted, allowing stabilization of the dihydroxo complex **2**. This conclusion is also supported by the structures of the corresponding Al^{III} and In^{III} complexes;[37] they are isostructural to **2**, indicating that crystal packing in this particular space group provides thermodynamic stability to the dihydroxo complexes of the $Hhbi^-$ ligand with trivalent metal ions. It would be of interest to verify whether or not the same chemistry takes place in the cases of the Al^{III} and In^{III} complexes but this is beyond the scope of the present work.

We suggest that the whole process involves protonation of one OH^- bridge toward an aquo ligand, which ceases to act as a bridge, and subsequent deprotonation of the remaining OH^- bridge toward an O^{2-} one. On the basis of the crystal packing, it may be proposed that the hydrogen-bonded water solvate molecule (O5) could act as a proton source for this process.

Supporting Information Available: Figures S1−S6 and crystallographic data in CIF format. This material is available free of charge via the Internet at http://pubs.acs.org.

IC800716R

(43) Hagen, W. R. *Mol. Phys.* **2007**, *105*, 2031.